5-2018

Phase field study of surface-induced melting and solidification from a nanovoid: Effect of dimensionless width of void surface and void size

Anup Basak
Iowa State University, abasak@iastate.edu

Valery I. Levitas
Iowa State University, vlevitas@iastate.edu

Phase field study of surface-induced melting and solidification from a nanovoid: Effect of dimensionless width of void surface and void size

Abstract
The size effect and the effects of a finite-width surface on barrierless transformations between the solid (S), surface melt (SM), and melt (M) from a spherical nanovoid are studied using a phase field approach. Melting (SM → M and S → M) from the nanovoid occurs at temperatures which are significantly greater than the solid-melt equilibrium temperature θe but well below the critical temperature for solid instability. The relationships between the SM and M temperatures and the ratio of the void surface width and width of the solid-melt interface, Δ——, are found for the nanovoids of different sizes. Below a critical ratio Δ——∗, the melting occurs via SM and the melting temperature slightly reduces with an increase in Δ——. Both S → SM and SM → M transformations have a jump-like character (excluding the case with the sharp void surface), causing small temperature hysteresis. However, the solid melts without SM for Δ——>Δ——∗, and the melting temperature significantly increases with increasing Δ——. The results for a nanovoid are compared with the melting/solidification of a nanoparticle, for which the melting temperatures, in contrast, are much lower than θe. A linear dependency of the melting temperatures with the inverse of the void radius is shown. The present study shows an unexplored way to control the melting from nanovoids by controlling the void size and the width and energy of the surface.

Keywords
phase transitions

Comments
This is the Accepted Manuscript of the article published as Basak, Anup, and Valery I. Levitas. "Phase field study of surface-induced melting and solidification from a nanovoid: Effect of dimensionless width of void surface and void size." *Applied Physics Letters* 112, no. 20 (2018): 201602. DOI: 10.1063/1.5029911. Posted with permission.

Phase field study of surface-induced melting and solidification from a nanovoid: effect of dimensionless width of void surface and void size

Anup Basak[1, a)] and Valery I. Levitas[2, b)]
[1)] *Department of Aerospace Engineering, Iowa State University, Ames, IA 50011, USA.*
[2)] *Departments of Aerospace Engineering, Mechanical Engineering, and Material Science and Engineering, Iowa State University, Ames, IA 50011, USA.*
Division of Materials Science and Engineering, Ames Laboratory, Ames, IA 50011, USA.

The size effect and the effects of finite-width surface on barrierless transformations between solid (S), surface melt (SM), and melt (M) from a spherical nanovoid are studied using a phase field (PF) approach. Melting (SM→M and S→M) from nanovoid occurs at temperatures which are significantly greater than the solid-melt equilibrium temperature θ_e but well below the critical temperature for solid instability. The relationships between the SM and M temperatures and the ratio of the void surface width and width of solid-melt interface, $\bar{\Delta}$, are found for the nanovoids of different sizes. Below a critical ratio $\bar{\Delta}^*$, the melting occurs via SM and the melting temperature slightly reduces with an increase in $\bar{\Delta}$. Both S→SM and SM→M transformations have a jump-like character (excluding the case with the sharp void surface), causing small temperature hysteresis. However, the solid melts without SM for $\bar{\Delta} > \bar{\Delta}^*$, and the melting temperature significantly increases with increasing $\bar{\Delta}$. The results for a nanovoid are compared with the melting/solidification of a nanoparticle, for which the melting temperatures, in contrast, are much lower than θ_e. A linear dependency of the melting temperatures with the inverse of the void radius is shown. The present study shows an unexplored way to control the melting from nanovoids by controlling the void size and the width and energy of the surface.

External and internal surfaces play an important role in the nucleation and kinetics of melting and solidification in materials[1]. Surface-induced surface melting, melting, and solidification are widely observed in nature and have great practical importance. For example, melting and surface melting are important in the combustion of nanoparticles[2]; surface melting increases the reactivity of explosives[3]; surface melting yields transformation of one solid into another, which would otherwise be impossible[4]; and melting temperatures in nanoparticles[5–15] and nanovoids[16] significantly differ from the thermodynamic equilibrium temperature between solid and melt, θ_e. The finite curvature of the surfaces plays an important role[15–18]. The surfaces reduce the melting temperature, θ_m, from the surface melt (SM) or solid to melt in nanoparticles well below θ_e (see e.g.[7,9–13,15]) and increase θ_m from nanovoids well above θ_e, allowing superheating of the solids (see e.g.[16,17]). Notably, θ_m is significantly lower than the instability temperature for solid at which barrierless transformation to melt occurs. For the particles embedded in the matrix, θ_m is smaller than θ_e[18].

Surface-induced melting in nanoparticles is well-understood based on the model with a sharp external surface[7–11,13,14]. Recently, however, multiple strong effects of finite-width of the surface were observed by utilizing the PF approach to lead to various counterintuitive phenomena[15]. It was shown that when the ratio $\bar{\Delta} = \delta_\xi/\delta$, where δ_ξ and δ are the widths of the surface and the solid-melt interface, respectively, is smaller than the critical value $\bar{\Delta}^*$, the melting occurs through the appearance of SM. However, above $\bar{\Delta}^*$ there is a discontinuity in the slope of the melting curve and the solid directly transforms to melt without SM. Also, the effect of size of the particle was investigated. However, we are not aware of any PF study on melting from nanovoids which are abundantly present in porous materials and are also often present in solids as defects. Few analytical studies have been conducted on melting of voids assuming the sharp void surface[17–23]. In these studies, the primary focus was to understand the reason behind the increase in melting temperatures of nanovoids. The stability of the melt layer on the void surface was studied in[24]. Molecular dynamics simulations were used to study the mechanism of melting in[16,24–27]. However, the effect of the width of void surface (i.e., internal surface) on void melting remains unexplored, and currently the only way to study it is to utilize the PF approach. Indeed, the phase field approach is currently the only method in which widths of the solid-melt interface δ and of the external surface δ_ξ can be directly included in the theory as physical parameters and their specific values can be prescribed and varied independent of any other parameter (e.g. interface energy). For comparison, in molecular dynamics simulations, the width of the external or internal surfaces and phase interface are not independent input parameters; they can be varied by changing parameters of the interatomic potential, which will change the other physical properties. Other continuum models such as the level set method[28] or the concentration based models for the microscale[29] consider the interfaces to be sharp ones with zero width, and hence not suitable for our objective. The authors are not aware of any other continuum or discrete models in which the interfaces can naturally

[a)] Electronic mail: anupbasak0@gmail.com
[b)] Electronic mail: vlevitas@iastate.edu

be modeled as diffused regions with prescribed widths.

Thus, the *goal* of this letter is to present the first PF study of melting at a nanovoid with focus on the effect of finite-width void surface and void radius. A melting temperature versus $\bar{\Delta}$ diagram is determined and analyzed in details. We show that with increasing $\bar{\Delta}$, below a critical $\bar{\Delta}^*$ the SM→M transformation temperature slightly decreases, but above $\bar{\Delta}^*$ the solid melts barrierlessly without surface melting and the melting temperature strongly increases. The SM→S and S→SM curves are also plotted. Within $0 < \bar{\Delta} \leq \bar{\Delta}^*$, the S→SM temperatures are slightly higher than the SM→S temperatures with a maximum difference of $2-3$ K, implying that these transformations yield hysteresis. The hysteresis is caused by discontinuous (jump-like) change in the stationary distribution of the order parameter during S→SM and SM→S transformations, excluding the case with $\bar{\Delta} = 0$. A similar jump exists for SM→M transformation. The effects of void size on melting, surface melting, and solidification are also analyzed. The melting temperatures and surface melting temperatures decrease with increase in the void size. The simulation result for melting of a nanoparticle is also presented and compared with the results for voids. In both the cases, the melting temperatures are well below the solid-to-melt instability temperature. While melting occurs significantly below θ_e for nanoparticles, it takes place significantly above θ_e for nanovoids.

Model. We have used a PF approach of the Ginzburg-Landau type[15], which considers an order parameter η for describing the solid↔melt transformations. An additional order parameter ξ is introduced to describe the transition between the material (solid or melt) and the surrounding (vacuum or gas), and thus introduce a finite width of the void surface S_0. The order parameter η is taken to be 0 in melt and 1 in solid, and $\xi = 0$ in the material and $\xi = 1$ in the surrounding.

The Helmholtz free energy per unit volume of the body is taken in the following form[15]

$$\psi(\eta,\xi,\theta,\nabla\eta,\nabla\xi) = \breve{\psi}^{\theta}(\eta,\theta) + \tilde{\psi}^{\theta}(\eta,\theta) + \psi^{\nabla}(\nabla\eta) + \psi_{\xi}(\eta,\xi,\nabla\xi), \quad (1)$$

where $\breve{\psi}^{\theta}$ is the barrier energy and $\tilde{\psi}^{\theta}$ is the thermal (or chemical) energy related to S↔M transformations, ψ^{∇} is the solid-melt gradient energy (∇ denotes the gradient operator), and ψ_{ξ} is the free energy related to S_0[15]:

$$\breve{\psi}^{\theta} = 3H(1-\theta_c^{MS}/\theta_e)\eta^2(1-\eta)^2, \quad \tilde{\psi}^{\theta} = H(\theta/\theta_e - 1)\varphi(\eta),$$
$$\psi^{\nabla} = 0.5\beta|\nabla\eta|^2, \quad \psi_{\xi} = A_{\xi}(\eta)\xi^2(1-\xi)^2 + 0.5\beta_{\xi}(\eta)|\nabla\xi|^2,$$
$$\text{where } \beta_{\xi}(\eta) = 1.084\,\delta_{\xi}\gamma_{\xi}(\eta), \quad A_{\xi}(\eta) = \frac{16.62\gamma_{\xi}(\eta)}{\delta_{\xi}}, \quad (2)$$

H is the heat of fusion, $\theta > 0$ is the absolute temperature, θ_c^{MS} and θ_c^{SM} are the critical temperatures for barrierless melt-to-solid and solid-to-melt transformations, respectively (i.e., when energy minimum for melt or solid disappears), $\beta > 0$ is the coefficient of gradient energy for S-M interface, $A_{\xi}(\eta)$ and $\beta_{\xi}(\eta)$, respectively, are the barrier energy coefficient and gradient energy coefficient of S_0, and the width of the void surface δ_{ξ} is defined as the distance between the points where $\xi = 0.05$ and $\xi = 0.95$. The interpolation function is $\varphi(\eta) = \eta^2(3-2\eta)$ which satisfies $\varphi(0) = 0$, $\varphi(1) = 1$, $\partial\varphi(0)/\partial\eta = \partial\varphi(1)/\partial\eta = 0$. The surface energy $\gamma_{\xi}(\eta)$ is taken as[14,15]

$$\gamma_{\xi}(\eta) = \gamma_l + (\gamma_s - \gamma_l)\varphi(\eta), \quad (3)$$

where γ_l and γ_s are the surface energies of the melt and solid, respectively. The Ginzburg-Landau equations describing the evolution of the order parameters are (also see[15])

$$\frac{\dot{\eta}}{L} = -\frac{\partial\psi}{\partial\eta} + \nabla\cdot\left(\frac{\partial\psi}{\partial\nabla\eta}\right) = -6H\left(\frac{\theta}{\theta_e}-1\right)(\eta-\eta^2) - 6H\left(1-\frac{\theta_c^{MS}}{\theta_e}\right)(\eta-3\eta^2+2\eta^3) - \frac{\partial\psi_{\xi}}{\partial\eta} + \beta\nabla^2\eta, \text{ and}$$
$$\frac{\dot{\xi}}{L_{\xi}} = -\frac{\partial\psi}{\partial\xi} + \nabla\cdot\left(\frac{\partial\psi}{\partial\nabla\xi}\right) = -2A_{\xi}(\xi-3\xi^2+2\xi^3) + \beta_{\xi}\nabla^2\xi, \quad (4)$$

where $L > 0$ and $L_{\xi} > 0$ are the kinetic coefficients for solid-melt interface and the surface S_0, respectively, and

$$\frac{\partial\psi_{\xi}}{\partial\eta} = \frac{\partial\gamma_{\xi}(\eta)}{\partial\eta}\left[\frac{16.62}{\delta_{\xi}}\xi^2(1-\xi)^2 + 0.542\delta_{\xi}|\nabla\xi|^2\right]. \quad (5)$$

When we consider the problem in a spherically-symmetric domain, the order parameters are functions of the radial coordinate r and independent of the azimuthal and zenith angles, and the problem can be solved in an one-dimensional domain $R \leq r < \infty$, where R is the initial void radius. Hence using the relations $\nabla^2(\cdot) = \frac{1}{r^2}\frac{\partial}{\partial r}(r^2\frac{\partial(\cdot)}{\partial r})$ and $|\nabla(\cdot)|^2 = (\partial(\cdot)/\partial r)^2$, the Ginzburg-Landau equations $(4)_{1,2}$ are simplified to

$$\frac{\dot{\eta}}{L} - \beta\frac{\partial^2\eta}{\partial r^2} = -6H\left(\frac{\theta}{\theta_e}-1\right)(\eta-\eta^2) - 6H\left(1-\frac{\theta_c^{MS}}{\theta_e}\right)\times (\eta-3\eta^2+2\eta^3) - \frac{\partial\psi_{\xi}}{\partial\eta} + \frac{2\beta}{r}\frac{\partial\eta}{\partial r}, \quad \text{and}$$
$$\frac{\dot{\xi}}{L_{\xi}} - \beta_{\xi}\frac{\partial^2\xi}{\partial r^2} = -2A_{\xi}(\xi-3\xi^2+2\xi^3) + \frac{2\beta_{\xi}}{r}\frac{\partial\xi}{\partial r}, \quad \text{where} \quad (6)$$

$$\frac{\partial\psi_{\xi}}{\partial\eta} = \frac{\partial\gamma_{\xi}(\eta)}{\partial\eta}\left[\frac{16.62}{\delta_{\xi}}\xi^2(1-\xi)^2 + 0.542\delta_{\xi}\left(\frac{\partial\xi}{\partial r}\right)^2\right] \quad (7)$$

The last terms in Eqs. $(6)_1$ and $(6)_2$ contribute to the evolution of the order parameters when the curvature $1/r$ is finite, as it is for particles or voids. Obviously, this term vanishes in a domain with a flat surface.

To study the effect of surface S_0 one should first solve Eq. $(6)_2$ to obtain the stationary distribution of ξ and then proceed to solve Eq. $(6)_1$ for η. Instead, we use the analytical stationary solution of Eq. $(6)_2$[15]

$$\xi = [1 + \exp\{5.54(R-r)/\delta_{\xi}\}]^{-1} \quad (8)$$

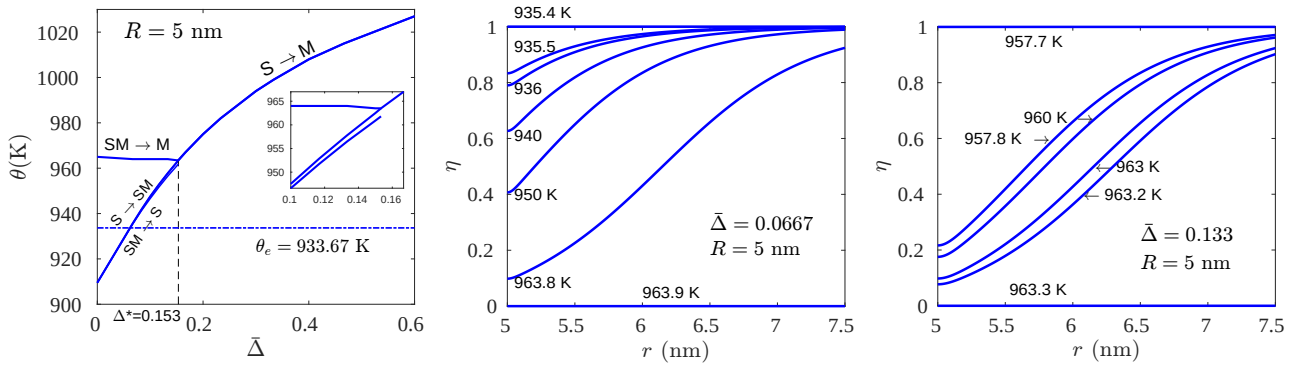

(a) (b) (c)

FIG. 1. (a) Temperature for barrierless transformations between SM, M, and S versus ratio $\bar{\Delta}$ of the width of the void surface to the width of S-M interface for a spherical void with 5 nm radius. (b) and (c) The stationary order parameter η profile for various temperatures between $\theta_{S\to SM}$ and θ_m for (b) $\bar{\Delta} = 0.0667$ and (c) $\bar{\Delta} = 0.133$.

in Eq. $(6)_1$ and then solve it, where R is the position where $\xi = 0.5$. We recall that $\xi = 1$ in the vacuum and $\xi = 0$ in the particle, and the stationary solution for ξ given by Eq. (8) is used such that half of the vacuum-particle interface is within $r < R$ and the other half lies in $r \geq R$ such that $\xi = 0.5$ at $r = R$. Here, we solve the Ginzburg-Landau equation Eq. $(6)_1$ in the computational domain $R \leq r \leq R_\infty$ using the finite element method[30] in the deal.ii[31], where $R_\infty \gg \delta_\xi$ is the external particle radius. Obviously, within our computational domain half of δ_ξ is present, within which we prescribe twice the surface energy and apply the Neumann boundary condition $\partial\eta/\partial r = 0$ at $r = R$. This is equivalent to considering the full surface width[15]. At $r = R_\infty$, we also take $\partial\eta/\partial r = 0$. The following material parameters for aluminum are used[14,15]: $H = 933.57\,\mathrm{MJ/m^3}$, $\theta_e = 933.67$ K, $\theta_c^{MS} = 746.9$ K, $\theta_c^{SM} = 1120.4$ K, $\beta = 3.21 \times 10^{-10}$ N, $\delta = 3$ nm, $L = 400\,\mathrm{m^2/Ns}$, $\gamma_s = 1.05$ N/m, $\gamma_l = 0.931$ N/m, and the solid-melt interfacial energy $\gamma_{sl} = 0.1$ N/m. The condition for surface melting at a sharp flat surface requires $\gamma_s - \gamma_l - \gamma_{sl} > 0$, and it is satisfied with the accepted energies. The results for $\bar{\Delta} = 0$ are obtained by using the PF model for a sharp interface[14] with corresponding boundary conditions.

Note that the solid-melt interface width $\delta = 3$ nm provides a good correspondence with the experiments on width of molten layer versus temperature for a planer Al surface; see[14]. The experimental results on size-dependence of the melting temperatures in Al nanoparticles were well-described by the present model with δ_ξ within the range 0.8-1.2 nm, i.e. for $0.27 \leq \bar{\Delta} \leq 0.4$ [15]. Because the width of the external and internal surfaces can be varied by changing the gaseous medium surrounding the surface, by surface alloying, or by a chemical reaction such as oxidation on the surface, we will vary $\bar{\Delta}$ between 0 and 0.6 to understand a general trend of the transformations. Then maximum δ_ξ considered here is thus 1.8 nm. As the lattice parameter of Al is 0.4 nm, the surface layer hence contains up to 4.5 atomic layers, which is reasonable (see e.g. Chapter 3 of[1]) and the range of $\bar{\Delta}$ is justified.

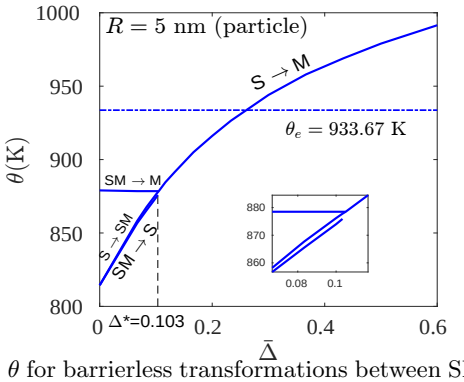

FIG. 2. θ for barrierless transformations between SM, M, and S versus $\bar{\Delta}$ for a spherical *particle* with 5 nm radius.

Numerical results and discussion. The transformation curves between SM, melt, and solid versus width ratio $\bar{\Delta}$ in a void with radius $R = 5$ nm is shown in Fig. 1(a), where we have taken $R_\infty = 40$ nm. To simulate solid to SM and to melt transformations, the initial condition for η is taken between 0.98 and 0.99, distributed randomly. There are two different melting regimes. For $\bar{\Delta} \leq \bar{\Delta}^* = 0.153$ the melting occurs through the appearance of SM, which is shown by the S→SM curve, corresponding to $\eta_R = 0.95$ at R. With increasing temperature, the value η_R reduces until the SM loses its stability at $\theta = \theta_m$ and the entire solid melts completely along the SM→M curve. The melting temperatures along the SM→M curve (for $0 \leq \bar{\Delta} \leq 0.153$) are approximately described by straight a line $\theta_m = (965 - 11.33\bar{\Delta})$ K, i.e., for the sharp surface and $\bar{\Delta} = 0.153$, melting occurs at 965 K and 963.3 K, respectively. However, at $\bar{\Delta} = 0.153$ there is a jump in the slope of the melting curve, and for $\bar{\Delta} > 0.153$ the solid directly transforms to complete

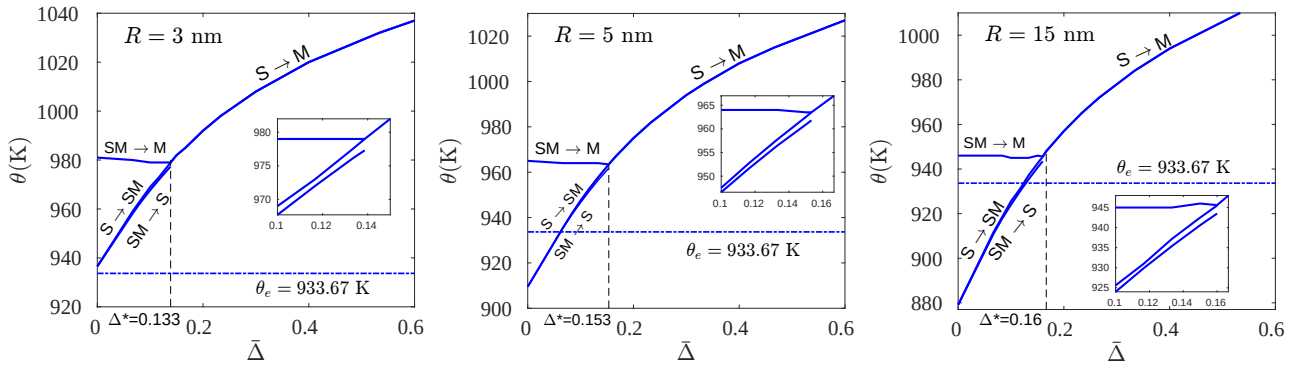

(a) (b) (c)

FIG. 3. (a) θ for barrierless transformations between SM, M, and S for voids with radius (a) 3 nm, (b) 5 nm, and (c) 15 nm.

melt without the appearance of any SM along the curve S→M. The melting temperature increases drastically for this range of $\bar{\Delta}$. Also, note that the melting points for all $\bar{\Delta} \geq 0$ are well above the bulk melting temperature $\theta_e = 933.67$ K, which confirms that the void allows superheating of the solid. The temperatures corresponding to SM→S and S→SM transformations coincide for the sharp interface ($\bar{\Delta} = 0$), but the SM→S transformation temperatures are slightly lower than the S→SM transformation temperatures for $\bar{\Delta} > 0$. The maximum difference in those temperatures is 1.6 K at $\bar{\Delta} = 0.153$, implying that there is a small hysteresis in S↔SM transformations. For $\bar{\Delta} > \bar{\Delta}^*$, the surface-melt is unstable and does not exist, and the entire particle is either in the solid phase or in the molten phase. That is why we have plotted the SM→S transformation curve within the range $0 \leq \bar{\Delta} \leq \bar{\Delta}^*$ only (see inset for a magnified view).

We have also calculated the melt→solid transformation temperatures for $0 \leq \bar{\Delta} \leq 0.6$ by considering the melt in a spherical region of radius 5 nm. The solidification temperature varies almost linearly according to $735.5 - 4.83\bar{\Delta}$ K, i.e. the temperature slightly decreases as $\bar{\Delta}$ increases.

The stationary profiles of the order parameters with varying temperatures between $\theta_{S\to SM}$ and θ_m are shown in Figs. 1(b) and 1(c) for $\bar{\Delta} = 0.0667$ and $\bar{\Delta} = 0.133$, respectively. For $\bar{\Delta} = 0.0667$, at $\theta = 935.4$ K the solution shows complete solid, but at $\theta = 935.5$ K there is a jump-like appearance of the surface melt within a narrow region. Such a jump like transformation is the reason for the small temperature hysteresis between the appearance and disappearance of the SM. As the temperature increases, the region over which the surface melt exists increases. There is a jump like transformation from SM to complete melt between $\theta = 963.8$ K and 963.9 K. Obviously, the range of temperatures over which the surface melt can exist decreases as the ratio $\bar{\Delta}$ increases, and the jump in the order parameter during S→SM transformation increases (Fig. 1(c)).

A comparative study between surface melting and melting in a nanovoid and a nanoparticle (Fig. 2), each having a radius of 5 nm, is now presented. Although the temperature plots in Figs. 1(a) and 2 possess similar qualitative features, including that all melting temperatures being well below the solid to melt instability temperature $\theta_c^{SM} = 1120.4$ K, there are subtle differences. The S→SM, SM→S, and S→M (for $\bar{\Delta} < 0.25$) temperatures are significantly lower than θ_e in the particle (see also[15]) in contrast to the void, for which the melting temperatures (SM→M and S→M) are much higher than θ_e over the entire range of $\bar{\Delta}$. This is in agreement with the results obtained earlier in[15,16,18,23,24,27]. Notably, the critical width ratio for the particle ($\bar{\Delta}^* = 0.103$) is smaller than that for the void ($\bar{\Delta}^* = 0.153$).

Let us discuss the effect of the void size on all the transformations. The melting temperatures versus $\bar{\Delta}$ plots for the voids with 3 nm, 5 nm, and 15 nm radius are shown in Fig. 3. Clearly, all the melting temperatures decrease towards θ_e as the void size increases. The difference between SM→M and S→SM transformation temperatures increases with increasing R over the entire $0 \leq \bar{\Delta} \leq \bar{\Delta}^*$ range. For instance, for 3 nm, 5 nm, and 15 nm voids the differences are 44.5 K, 55.5 K, and 63.4 K, respectively, for $\bar{\Delta} = 0$. The critical thickness ratio $\bar{\Delta}^*$ increases in larger voids.

In Fig. 4 the plots are shown for S→SM and SM→M transformation temperatures for $\bar{\Delta} = 0.1$ and S→M transformation temperatures for $\bar{\Delta} = 0.3$ for voids with varying size. Obviously, all of the transformation temperatures increase with decreasing R and vary linearly with $1/R$.

Our results for the nanovoids are qualitatively in agreement with the atomistic simulation results of[16], where it was reported that the melting temperature in nanovoids are above the bulk melting point and the melting starts at that surface through the appearance of surface-melt. The linear decrease in transformation temperatures with $1/R$ is also in agreement with thermodynamic studies[20] and atomistic simulations[16]. The validity of the current model was confirmed in[15], where the experimental results

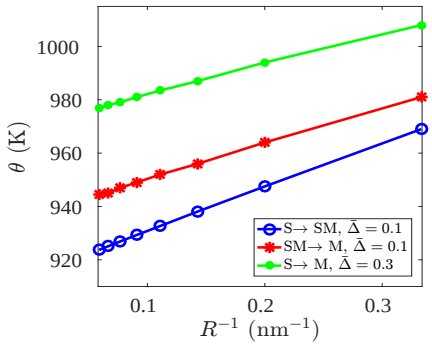

FIG. 4. Variation of S→SM and SM→M transformation temperatures for $\bar{\Delta} = 0.1$ and S→M transformation temperatures for $\bar{\Delta} = 0.3$ with $1/R$. Obviously, θ is linear in R^{-1}.

of melting in a nanoparticle were reproduced. However, we are not aware of any suitable experimental/atomistic simulation data which can be directly used here for a quantitative comparison with the current results for a nanovoid. We hope that our predictions will encourage a systematic experimental and/or atomistic study to understand the role of surface width in the solid↔melt transformations in nanovoids.

In summary, we have presented the first PF study of the barrierless transformations between solid, surface melt, and melt in the nanovoids. The key effects are caused by the ratio $\bar{\Delta}$ of the width of the void surface and solid-melt interface and by the void size. There are two different melting regimes. During heating for $\bar{\Delta} \leq \bar{\Delta}^*$, surface melt appears in a jump-like process, grows, loses its stability, and undergoes a jump-like transformation to complete melt. For $\bar{\Delta} > \bar{\Delta}^*$, surface melt does not appear and the solid melts directly. The melting temperatures for voids are much higher than θ_e, in contrast to the particles for which the melting temperatures are much smaller than θ_e. A jump-like process explains the hysteresis between the appearance and disappearance of the surface melt, but it is only a few degrees. For the void with a sharp surface, the jump and hysteresis are absent. With increasing $\bar{\Delta}$, the melting temperature slightly decreases for $\bar{\Delta} \leq \bar{\Delta}^*$ and strongly increases for $\bar{\Delta} > \bar{\Delta}^*$. With increasing void radius, all of the melting temperatures decrease toward θ_e; the difference between SM→M and S→SM transformation temperatures and the critical thickness ratio $\bar{\Delta}^*$ both increase. Our study demonstrates a direction to control the melting of solids by controlling the size of voids and the energy and width of the void surfaces. For example, (i) one can change the gaseous medium surrounding a particle or the gaseous medium within an open system of voids. (ii) Alloying the void surfaces by different elements would changes their widths and energy. (iii) The void surfaces can be deformed plastically by generating defects therein. The generated stresses can modify the surface width in some materials[32]. (iv) A surface reaction, such as oxidation, is another way to engineer the surface energy and width.

Note that the ratio of two nanoscale parameters strongly affects material behavior in martensitic transformations[33], interaction between phase transformation and dislocations[34], and solid-solid phase transformation via intermediate melt[35,36]; see[37] for a review.

Acknowledgments. Support from ONR (N00014-16-1-2079), NSF (CMMI-1536925 and DMR-1434613), and Iowa State University (Vance Coffman Faculty Chair Professorship) is gratefully acknowledged.

[1]D.A. Porter, K.E. Easterling, M.Y. Sherif, Phase Transformations in Metals and Alloys. (CRC Press, Boca Raton, 2009).
[2]V.I. Levitas, Phil. Trans. Royal Society A 371 (2013) 20120215.
[3]B. F. Henson, L. Smilowitz, 14th International Detonation Symposium, Coeur dAlene, Idaho (https://getinfo.de/app/The-Surface-Quasiliquid-Melt-Acceleration-and-the/id/BLCP%3ACN080849513, 2010).
[4]V.I. Levitas, Z. Ren, Y. Zeng, Z. Zhang, G. Han, Phys. Rev. B 85 (2012) 220104.
[5]C.R.M. Wronski, Brit. J. Appl. Phys. 18 (1967) 1731-1737.
[6]C.J. Coombes, J. Phys. F: Metal Phys. 2 (1972) 441-449.
[7]R.P. Berman, A.E. Curzon, Canad. J. Phys. 52 (1974) 923-929.
[8]P.R. Couchman, W.A. Jesser, Nature 269 (1977) 481-483.
[9]R. Lipowsky, Phys. Rev. Lett. 323 (1982) 1575-1578.
[10]R.W. Cahn, Nature 323 (1986) 668-669.
[11]G.L. Allen, R.A. Bayles, W.W. Gile, W.A. Jesser, Thin Solid Films 144 (1986) 297-308.
[12]H. Löwen, R. Lipowsky, Phys. Rev. B 43 (1991) 3507-3513.
[13]F. Ercolessi, W. Andreoni, E. Tosatti, Phys. Rev. Lett. 66 (1991) 911-914.
[14]V.I. Levitas, K. Samani, Nat. Commun. 2, 284 (2011).
[15]V.I. Levitas, K. Samani, Phys. Rev. B 89 (2014) 075427.
[16]X.M. Bai, M. Li, Nano Lett. 6 (2006) 2284-2289.
[17]H.M. Lu, D.N. Ding, Z.H. Cao, S.C. Tang, X.K. Meng, J. Phys. Chem. C 111 (2007) 12914-12917.
[18]R. Kofman, P. Cheyssac, A. Aouaj, Y. Lereah, G. Deutscher, T. Ben-Davida, J.M. Penissonc, A.Bourret, Surf. Sci. 303 (1994) 231-246.
[19]Z.H. Liu, H. Li, L.S. Yang, Physica B 405 (2010) 4863-4865.
[20]H. Li, Z. Wen, Q. Jiang, Solid State Comm. 147 (2008) 250-253.
[21]S. Xiong, W. Qi, Y. Cheng, B. Huang, M. Wang, Y. Li, Phys. Chem. Chem. Phys. 13 (2011) 10648-10651.
[22]G. Ouyang, X.L. Li, G.W. Yang, Appl. Phys. Lett. 92 (2008) 051902.
[23]G. Ouyang, C.X. Wang, G.W. Yang, Chem. Rev. 109 (2009) 4221-4247.
[24]H. Li, X.H. Liang, M. Li Mater. Chem. Phys. 144 (2014) 390-395.
[25]S. Li, W. Qi, J. Phys. Chem. C 119 (2015) 6843-6851.
[26]He, A. M., Duan, S., Shao, J. L. J. Appl. Phys. 112 (2012) 074116.
[27]P.M. Agrawal, B.M. Rice, D.L. Thompson, J. Chem. Phys. 118 (2003) 9680-9688.
[28]A. Basak, A. Gupta, Model. Simul. Mater. Sci. Eng. 22 (2014) 055022.
[29]A.V. Idesman, V.I. Levitas, D.L. Preston, J.Y. Cho, J. Mech. Phys. Solids 53 (2005) 495-523.
[30]O.C. Zienkiewicz, R.L. Taylor, The Finite Element Method: Volume 1- The Basis, (Butterworth-Heinemann, Woburn, 2000).
[31]W. Bangerth, D. Davydov, T. Heister, L. Heltai, G. Kanschat, M. Kronbichler, M. Maier, B. Turcksin, D. Wells, J. Numer. Math. 24 (2016).
[32]V.I. Levitas, H. Chen, L. Xiong, Phys. Rev. Lett. 118 (2017) 025701.
[33]V.I. Levitas, M. Javanbakht, Phys. Rev. Lett. 107 (2011) 175701.
[34]V.I. Levitas, M. Javanbakht, Appl. Phys. Lett. 102 (2013) 251904.
[35]V.I. Levitas, K. Momeni, Acta Mater. 65 (2014) 125-132.
[36]V.I. Levitas, A.M. Roy, Acta Mater. 105 (2016) 244-257.
[37]V.I. Levitas, Scripta Mater. 149C (2018) 155-162.